Available online at www.sciencedirect.com
SCIENCE DIRECT®
Journal of Sound and Vibration 284 (2005) 1075–1097
JOURNAL OF SOUND AND VIBRATION
www.elsevier.com/locate/jsvi

On the linear normal modes of planar pre-stressed curved beams

D. Addessi, W. Lacarbonara*, A. Paolone

Dipartimento di Ingegneria Strutturale e Geotecnica, University of Rome La Sapienza, via Eudossiana 18, Rome 00184, Italy

Received 14 August 2003; received in revised form 1 July 2004; accepted 27 July 2004
Available online 24 November 2004

Abstract

The natural frequencies and mode shapes of planar shear undeformable beams around their curved pre-stressed post-buckling configurations are investigated neglecting rotary inertia effects. Two mechanical models are considered depending on the assumed boundary conditions in the buckling and post-buckling phases. With the first model, the beam is considered inextensible because it is hinged at one end and is acted upon by an axial compressive force on the other end, a sliding hinge. In the second case, the beam is assumed inextensible in the pre-stressed phase (same boundary conditions as above), whereas it is extensible in the subsequent free linear dynamic phase because the sliding hinged boundary is changed into a stationary hinged end. Linear vibrations are governed by partial-differential equations with non-constant coefficients and the solutions for the frequencies and mode shapes are found employing two approximate approaches: a fully numerical method based on a finite element formulation and a semi-analytical method based on a weak formulation (Galerkin method). The main results are compared and a close agreement in the outcomes is found. The leading mechanical differences in the linear normal modes of the two pre-stressed curved beam models are discussed.

*Corresponding author. Tel.: +39 6 44 585 293; fax: +39 6 488 4852.
E-mail address: walter.lacarbonara@uniroma1.it (W. Lacarbonara).

0022-460X/$ - see front matter © 2004 Elsevier Ltd. All rights reserved.
doi:10.1016/j.jsv.2004.07.021

1. Introduction

Linear vibrations of planar curved beams, arches and rings have been the subject of numerous studies due to their extensive use in a wide variety of engineering applications such as bridges, aircraft structures, and turbo-machinery blades. These structures are modelled as either extensional (including the extension of the neutral axis) or inextensional Euler–Bernoulli and Timoshenko curved beams. Literature reviews on vibrations of curved beams, rings and arches are found in Refs. [1,2].

Several methods have been employed to study free vibrations of curved beams. Den Hartog [3] obtained the natural frequencies of circular arches with fixed and hinged boundary conditions using the Rayleigh–Ritz method. On the other hand, Rao and Sundararajan [4] and Tufekci and Arpaci [5] solved the equations of motion governing in-plane vibrations with classical boundary conditions. Chidamparam and Leissa [6] used the Galerkin method to study in-plane free vibrations of extensional and inextensional loaded circular arches. Mau and Williams [7] solved the arch vibration problem using the Green function.

Numerous studies have developed beam finite elements for both Timoshenko and Euler–Bernoulli curved beam models, among them, the works of Petyt and Fleischer [8], Prathap [9], and Yang and Sin [10]. Grosh and Pinsky [11] implemented the Galerkin generalized least-squares method to solve for the steady-state responses of Timoshenko beams and arches.

Kang et al. [12] used the differential quadrature method to compute the eigenvalues of the equations of motion governing free in-plane vibrations, including extensibility of the arch axis and the coupled out-of-plane twist-bending vibrations of circular arches. In-plane buckling and twist-buckling under uniformly distributed radial loads were also investigated for clamped and simply supported boundary conditions. They found a good agreement with the results obtained with other methods using a limited number of grid points.

Matsunaga [13] employed the method of power series expansion of the displacement components and Hamilton's principle to derive a set of equations of motion of a one-dimensional higher-order theory for in-plane vibrations of shallow circular arches. He analyzed the natural frequencies and buckling loads of a simply supported shallow arch subjected to axial compressive forces, accounting also for shear deformations and rotary inertia.

Oh et al. [14] derived the differential equations governing free in-plane vibrations of non-circular arches with non-uniform cross sections and solved them numerically to obtain the frequencies and mode shapes. Numerical results were presented for the quadratic, parabolic, catenary and elliptic arches with hinged–hinged, hinged–clamped, and clamped–clamped boundary conditions and for three general taper-type rectangular sections. They also presented experimental measurements of the natural frequencies and mode shapes and showed a close agreement with those predicted by the theory.

Perkins [15] examined the planar, linear vibrations of a simply supported non-shallow arch formed of a rod that buckles nonlinearly under the action of a compressive end load. He employed the geometrically nonlinear rod theory to describe the planar bending of the rod. Subsequent to buckling, he considered stationary hinged ends. He used a variational formulation to solve the eigenvalue problem for the natural frequencies and mode shapes of vibration around an elastica equilibrium. The stationary hinges allowed to use the sine series as admissible functions. He found good agreement with the experimental results relating to the lowest two frequencies and mode shapes.

A large number of works has dealt with shallow pre-stressed arch models using the approximate theory due to Mettler [16]. In Mettler's theory, the arch bending curvature is linear, whereas the centerline stretching is nonlinearly related to the transverse deflection and a condensation procedure is used to obtain the governing equation of motion in the transverse direction. This theory has been used to model also buckled beams, although restricted to shallow post-buckling configurations. Both the linear [17] and nonlinear [18] vibration regimes of buckled beams have been investigated analytically and experimentally, with an overall good agreement between theory and experiments.

It is worth noting that Mettler's shallow arch theory is applicable only to beams and arches that are statically indeterminate in the longitudinal direction, such as hinged–hinged or fixed–fixed beams. Nonetheless, there is a clear theoretical as well as a practical interest for investigating different boundary conditions and non-shallow pre-stressed configurations with the appropriate mechanical formulation. On a merely theoretical ground, it is well known that the post-buckling problem of the Euler rod plays the role of a mechanical paradigm for static and dynamical critical and post-critical scenarios [19]. It has also been shown experimentally that a wealth of nonlinear phenomena occurs in systems such as simply supported beams in their non-shallow post-buckling regimes [20].

From a practical point of view, there are at least three areas of engineering interest: (i) vibration isolation, (ii) mechanical actuation and (iii) aircraft design. In the field of vibration isolation, the concept is to interject, between the primary structure and the excitation source, a buckled mechanism possessing a low fundamental frequency right above buckling [21,22].

Further, the fact that small longitudinal displacements of the boundary of a buckled beam cause large rotations of the end section makes a buckled beam or structure an effective mechanical amplifier, hence, a rotary actuator [23]. Finally, in current aircraft industry the major challenge is to design light-weight structural components that can accordingly be allowed to buckle under some loading conditions. Hence, it is critical to predict with high accuracy their static and dynamic post-buckling behavior.

To describe the dynamics of generally constrained non-shallow pre-stressed elastica systems, a geometrically exact approach has been employed in Ref. [24]. In the present paper, the linearization of the governing equations is performed and two leading mechanical models are constructed, namely, the Kirchhoff and Euler–Bernoulli rods. Further, for each mechanical model, both finite element and semi-analytical approaches are used. The objective is to study the sensitivity of the modal properties in the vicinity of the first buckling Euler load. For both models, appropriate admissible functions are used in the weak formulation based on Galerkin's method [25] in order to obtain the natural frequencies and mode shapes. More specifically, the motivation for constructing closed-form expressions for the mode shapes is connected with the need of a basis for analytically studying the nonlinear post-critical responses to external resonant excitations both for auto-parametric and non-auto-parametric conditions.

2. Problem formulation and computational schemes

In this section, the mechanical models describing the free vibration problem of pre-stressed planar curved beams with different post-buckling boundary conditions are illustrated. The beams,

made of a homogeneous isotropic and hyper-elastic material and naturally resting with an initial simply supported configuration, are subjected to a longitudinal end load monotonically increasing beyond the first critical Eulerian value; subsequently, the post-buckling free linear dynamical behavior is analyzed. In particular, two post-buckling configurations are investigated: the simply supported configuration—same boundary conditions as in the buckling phase—and the hinged–hinged configuration whereby the right sliding hinge is turned into a stationary [15] hinged end.

The extended theoretical formulation of the exact mechanical model for nonlinear planar motions around non-shallow pre-stressed states is discussed in Ref. [24]. The Kirchhoff's hypotheses of inextensibility and unshearability are assumed during the static pre-buckling deformation process. This assumption is well established in the literature for slender rods [19]; in fact, it can be shown that the effect of shear deformations on the overall elastic deformation process is negligible. At the same time, when the beam is statically determinate in the axial direction, axial deformations can be neglected with respect to bending deformations for typical material properties and loading conditions. Hence, during the small-amplitude post-buckling motions, Kirchhoff's hypotheses hold for the simply supported configuration, whereas the inextensibility assumption is removed for the hinged–hinged case.

The pre-stressed equilibrium state C_0 (Fig. 1), described by the displacement vector $\mathbf{u}_0$, with respect to the straight undeformed beam axis C_n is adopted as initial reference configuration for the motions around it, whereby the beam section position is described by the coordinate x measured along C_n. Hence, the elastodynamic problem is parameterized by $x \in [0, \ell]$ (ℓ is the length of the undeformed beam) and the planar dynamic configuration C is described by the vector $\mathbf{u}$ whose components, in the local basis, are (u, v) (Fig. 1).

Denoting with $\mathbf{t}_0(x)$ and $\mathbf{m}_0(x)$ the resultant contact force and contact couple, respectively, acting between two adjoining material sections originally located at x in the reference configuration, the balance of linear momentum and angular momentum in the pre-stressed configuration can be expressed as

$$\mathbf{t}_0' + \mathbf{b}_0 = \mathbf{0}, \quad \mathbf{m}_0' + \mathbf{x}_0' \times \mathbf{t}_0 = \mathbf{0}, \tag{1}$$

where $\mathbf{x}_0$ is the position vector of the beam section in C_0. The mechanical boundary conditions are

$$\mathbf{t}_0 = \mp \mathbf{B}_0, \quad \mathbf{m}_0 = \mp \mathbf{C}_0 \quad \text{at } x = 0, \ell \tag{2}$$

where the prime indicates differentiation with respect to x, $\mathbf{b}_0$ is the vector of the body forces per unit undeformed reference length, $\mathbf{B}_0$ and $\mathbf{C}_0$ denote the boundary forces and couples, respectively; the minus sign corresponds to $x = 0$ and the plus sign to $x = \ell$.

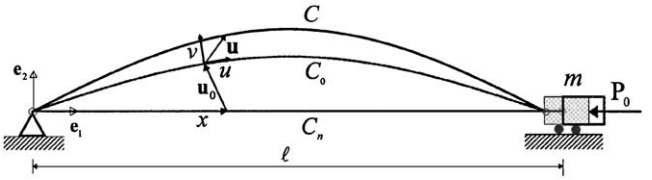

Fig. 1. Schematic geometry of the simply supported buckled beam.

Accounting for Eq. (1), the balance equations in the dynamic configuration C are

$$\mathbf{t}' + \mathbf{b} = \mathbf{0}, \tag{3}$$

$$\mathbf{m}' + \mathbf{x}' \times \mathbf{t} + \mathbf{u}' \times \mathbf{t}_0 = \mathbf{0} \tag{4}$$

and

$$\mathbf{t} = \mp\mathbf{B}, \quad \mathbf{m} = \mp\mathbf{C} \quad \text{at } x = 0, l, \tag{5}$$

where $\mathbf{x}$ is the position vector of the beam section in C, $\mathbf{t}$ and $\mathbf{m}$ are the incremental resultant contact force and couple, $\mathbf{b}$ represents the body forces per unit reference length (here inertial forces only). Neglecting the rotary inertia, the scalar equations of motion governing free planar vibrations of pre-stressed curved beams become

$$N' - \theta_0' T - \rho A \ddot{u} = 0, \tag{6}$$

$$T' + \theta_0' N - \rho A \ddot{v} = 0, \tag{7}$$

$$M' + T - N_0 \theta = 0, \tag{8}$$

where N and T represent the incremental axial and shear forces, and M is the incremental bending moment; $\theta = (v' + \theta_0' u)$ is the incremental dynamic section rotation; ρ is the mass density and A the area of cross section; the dot denotes differentiation with respect to time t. At the same time, θ_0 is the beam section rotation from C_n to C_0, hence $\kappa_0 = \theta_0'$ denotes the bending curvature in the initial pre-stressed configuration C_0 and N_0 indicates the axial force (i.e., pre-stress). Considering the simply supported beam acted upon by an end longitudinal load P_0, accounting for Eq. (1) and $N_0 = -P_0 \cos\theta_0$, the following nonlinear boundary-value problem is obtained in the unknown rotation θ_0:

$$EJ\theta_0'' + P_0 \sin\theta_0 = 0, \tag{9}$$

along with the boundary conditions $EJ\theta_0' = 0$ at $x = 0$ and $x = \ell$ representing the moment-free end supports. Eq. (9) represents the well-known elastica problem [26] which holds for more general boundary conditions. Typically, in this equation the arch-length along the deformed beam centerline is taken as independent space variable. However, as shown also in Ref. [27] when the beam is inextensible, it is immaterial to use the arch-length or the x coordinate along the centerline of the undeformed beam.

In Eq. (9), the linear constitutive law, $M_0 = EJ\kappa_0$, relating the bending moment to the bending curvature κ_0 was used, whereby E is Young's modulus, J is the moment of inertia of the undeformed cross section. The solutions of the elastica problem can be expressed using elliptic integrals [15,26]. On the other hand, making use of a perturbation method, an asymptotic expression of the fundamental post-buckling solution was found in Ref. [20] in the form, up to fifth order,

$$\theta_0(x) = \hat{\theta}_0 \cos(\pi x) - \frac{\hat{\theta}_0^3}{192} \cos(3\pi x) - \frac{\hat{\theta}_0^5}{20{,}480}[-5\cos(3\pi x) + \cos(5\pi x)] \tag{10}$$

along with the expansion of the end load P_0 expressed as

$$\frac{P_0 l^2}{EJ} = \pi^2 + \frac{\pi^2}{8}\hat{\theta}_0^2 + \frac{5\pi^2}{512}\hat{\theta}_0^4 + \cdots,$$

where $\hat{\theta}_0$ is a small parameter, indicating the rotation of the end sections to first order.

In Eqs. (6)–(8), the shear force is treated as a reaction force, since the considered beams are unshearable and is filtered out of the balance equations. The result is

$$\begin{aligned} \rho A\ddot{u} - N' - \theta_0' M' + N_0\theta_0'\theta = 0, \\ \rho A\ddot{v} + M'' - \theta_0' N - N_0\kappa - N_0'\theta = 0. \end{aligned} \tag{11}$$

The beam linearized strain measures, the axial strain and the bending curvature, are expressed in terms of the kinematic variables (u, v) as

$$\varepsilon = u' - \theta_0' v, \quad \kappa = v'' + \theta_0'' u + \theta_0' u'. \tag{12}$$

The dynamic incremental axial force and bending moment are related to the dynamic axial strain and bending curvature by the following linear constitutive laws:

$$N = EA\varepsilon, \quad M = EJ\kappa.$$

In the next sections, the two post-buckling static configurations are separately discussed; namely, the simply supported and hinged–hinged cases.

2.1. The simply supported case

Considering the beam in Fig. 1, the kinematical and mechanical boundary conditions assume, respectively, the forms

$$\begin{aligned} &u = 0 \quad \text{and} \quad v = 0 \quad \text{at } x = 0, \\ &u \sin\theta_0 + v\cos\theta_0 = 0 \quad \text{at } x = \ell, \end{aligned} \tag{13}$$

$$\begin{aligned} &M = 0 \quad \text{at } x = 0, \\ &M = 0 \quad \text{and} \quad N\cos\theta_0 - T\sin\theta_0 = -m(\ddot{u}\cos\theta_0 - \ddot{v}\sin\theta_0) \quad \text{at } x = \ell. \end{aligned} \tag{14}$$

The last boundary condition in Eq. (14) is obtained from the balance equation $\mathbf{t}\cdot\mathbf{e}_1 = \mathbf{B}\cdot\mathbf{e}_1$, where $\mathbf{t}$ is the internal contact force and $\mathbf{B} = -m\ddot{\mathbf{u}}$ at $x = \ell$. Here m (see Fig. 1) indicates the boundary lumped mass element, where the physical actuator force P_0 is applied. Due to Kirchhoff's hypotheses, the longitudinal displacement u and the dynamic bending curvature κ can be expressed as functions of the transverse displacement v only in the form

$$u = \int_0^x \theta_0' v \, d\eta, \quad k = v'' + \theta_0'' \int_0^x \theta_0' v \, d\eta + \theta_0'^2 v, \tag{15}$$

where use of Eq. (13_1) has been made.

Since the reactive axial force N is known at $x = \ell$, it can be obtained integrating Eq. (6). In fact, using Eq. (14_2) and introducing the shear force T from Eq. (8) yields

$$N = N(l) - \int_x^l N_0\theta_0' v' \,\mathrm{d}\eta - \int_x^l N_0\theta_0'^2 \left(\int_0^\eta \theta_0' v \,\mathrm{d}\xi\right)\mathrm{d}\eta + \int_x^l \theta_0' M' \,\mathrm{d}\eta - \int_x^l \rho A \left(\int_0^\eta \theta_0' \ddot{v} \,\mathrm{d}\xi\right)\mathrm{d}\eta, \tag{16}$$

where

$$N(l) = N_0(l)v'(l)\tan\theta_0(l) - M'(l)\tan\theta_0(l) - m\int_0^l \theta_0'\ddot{v}\,\mathrm{d}x + m\ddot{v}(l)\tan\theta_0(l). \tag{17}$$

As a consequence of the internal kinematic constraints, the only internal active force is the bending moment, M, and the balance equations (6)–(8) can be reduced to one equation only in the transverse unknown displacement v. Using the mentioned constitutive laws, the dimensional equation of motion governing transverse vibrations can be written as

$$\begin{aligned}
&\rho A\ddot{v} + \theta_0' \int_x^l \rho A\left(\int_0^\eta \theta_0'\ddot{v}\,\mathrm{d}\xi\right)\mathrm{d}\eta + m\theta_0' \int_0^l \theta_0'\ddot{v}\,\mathrm{d}x - m\theta_0'\ddot{v}(l)\tan\theta_0(l)\\
&+ EJ\left(v'''' + \theta_0'''' \int_0^x \theta_0' v\,\mathrm{d}\eta + 4\theta_0'\theta_0''' v + 3\theta_0''^2 v + 5\theta_0'\theta_0'' v' + \theta_0'^2 v''\right)\\
&+ EJ\theta_0'\tan\theta_0(l)\left(v'''(l) + \theta_0'''(l)\int_0^l \theta_0' v\,\mathrm{d}x\right)\\
&- \theta_0' \int_x^l \theta_0' EJ\left(v''' + \theta_0''' \int_0^\eta \theta_0' v\,\mathrm{d}\xi + 3\theta_0'\theta_0'' v + \theta_0'^2 v'\right)\mathrm{d}\eta\\
&+ P_0\left[\theta_0' v'(l)\sin\theta_0(l) - \theta_0' \int_x^l \theta_0'\cos\theta_0 v'\,\mathrm{d}x - \theta_0' \int_x^l \theta_0'^2\cos\theta_0\left(\int_0^\eta \theta_0' v\,\mathrm{d}\xi\right)\mathrm{d}\eta\right.\\
&\left.- \theta_0'\sin\theta_0\left(v' + \theta_0'\int_0^x \theta_0' v\,\mathrm{d}\eta\right) + \cos\theta_0\left(v'' + \theta_0''\int_0^x \theta_0' v\,\mathrm{d}\eta + \theta_0'^2 v\right)\right] = 0.
\end{aligned} \tag{18}$$

A non-dimensional form of Eq. (18) can be obtained introducing the following variables:

$$t^* = \omega_c t, \quad x^* = \frac{x}{\ell}, \quad v^* = \frac{v}{l}, \quad P_0^* = \frac{P_0\ell^2}{EJ}, \quad \mu = \frac{m}{\rho A\ell}, \tag{19}$$

where $\omega_c = \sqrt{(EJ)/(\rho A\ell^4)}$.

Then, Eq. (18) can be cast in compact form as

$$\mathscr{I}(\ddot{v}) + \mathscr{L}_E(v) + P_0\mathscr{L}_G(v) = 0, \tag{20}$$

where the inertial ($\mathscr{I}$), elastic ($\mathscr{L}_E$) and geometric ($\mathscr{L}_G$) stiffness operators take the following forms:

$$\mathscr{I} = \ddot{v}(x,t) + \theta_0' \int_x^1 \left(\int_0^\eta \ddot{v}(\xi,t)\theta_0'\,\mathrm{d}\xi\right)\mathrm{d}\eta - 2\mu\theta_0' \frac{\ddot{v}(1,t)}{\sin 2\theta_0(1)}, \tag{21}$$

$$\mathscr{L}_E = v'''' + \theta_0'''' \int_0^x \theta_0' v \, \mathrm{d}\eta + 4\theta_0'\theta_0''' v + 3\theta_0''^2 v + 5\theta_0'\theta_0'' v' + \theta_0'^2 v'' + \theta_0' \tan\theta_0(1) \times \left(v'''(1,t) + \theta_0'''(1) \int_0^1 \theta_0' v \, \mathrm{d}x \right) - \theta_0' \int_x^1 \theta_0' \left(v''' + \theta_0''' \int_0^\eta \theta_0' v \, \mathrm{d}\xi + 3\theta_0'\theta_0'' v + \theta_0'^2 v' \right) \mathrm{d}\eta, \quad (22)$$

$$\mathscr{L}_G = \theta_0' v'(1,t) \sin\theta_0(1) - \theta_0' \int_x^1 \theta_0' \cos\theta_0 v' \, \mathrm{d}\eta - \theta_0' \int_x^1 \theta_0'^2 \cos\theta_0 \left(\int_0^\eta \theta_0' v \, \mathrm{d}\xi \right) \mathrm{d}\eta - \theta_0' \sin\theta_0 \left(v' + \theta_0' \int_0^x \theta_0' v \, \mathrm{d}\eta \right) + \cos\theta_0 \left(v'' + \theta_0'' \int_0^x \theta_0' v \, \mathrm{d}\eta + \theta_0'^2 v \right). \quad (23)$$

In Eqs. (20)–(23), the prime and dot denote differentiation with respect to the non-dimensional coordinate x^* and non-dimensional time t^*. However, the star has been omitted for ease of notation. The PDE boundary-value problem (20) is supplemented with the following geometric and mechanical boundary conditions:

$$v = 0 \quad \text{at } x = 0,$$
$$\int_0^1 \theta_0' v \, \mathrm{d}x \sin\theta_0 + v \cos\theta_0 = 0 \quad \text{at } x = 1 \quad (24)$$

and

$$v'' = 0 \quad \text{at } x = 0$$
$$v'' + \theta_0'' \int_0^1 \theta_0' v \, \mathrm{d}x = 0 \quad \text{at } x = 1, \quad (25)$$

The eigenvalue problem (20), (24), (25) is solved assuming, first, separable solutions, i.e. $v(x,t) = V(x)\mathrm{e}^{\mathrm{i}\omega t}$ and, secondly, putting

$$V(x) \approx \sum_{k=1}^{M} X_k [\sin(k\pi x) + y_k(x)], \quad (26)$$

where

$$y_k(x) = \left(C_{1k} - \frac{C_{2k}}{6} \right) x + \frac{C_{2k}}{6} x^3 \quad (27)$$

is determined such that $V(x)$ satisfies all of the boundary conditions. The derivation of y_k and the coefficients C_{1k} and C_{2k} are given in Appendix A.

The approximate solution (26) is introduced into the inertial and stiffness operators (21), (22) and (23) and the Galerkin method [25] is applied to Eq. (20), using the following trial functions as weighting functions:

$$f_j^*(x) = \sin(\mathrm{j}\pi x) + y_j(x). \quad (28)$$

Thus, a set of M equations in the unknown X_k is obtained. The discretized forms of the inertial and stiffness operators are reported in Appendix A.

2.2. The hinged–hinged case

Due to the stationary hinges in the post-buckling phase (Fig. 2), the beam cannot be considered inextensible; therefore, two coupled equations of motion govern the equilibrium in the axial and transverse directions. They are formally identical to Eq. (20), where the inertial and stiffness operators become

$$\mathbf{I} = \begin{Bmatrix} \ddot{u} \\ \ddot{v} \end{Bmatrix}, \tag{29}$$

$$\mathbf{L}_E = \begin{Bmatrix} -\lambda^2(u'' - \theta_0''v - \theta_0'v') - \theta_0'(v''' + \theta_0'''u + 2\theta_0''u' + \theta_0'u'') \\ v'''' + \theta_0''''u + 3\theta_0'''u' + 3\theta_0''u'' + \theta_0'u''' - \lambda^2\theta_0'(u' - \theta_0'v) \end{Bmatrix}, \tag{30}$$

$$\mathbf{L}_G = \begin{Bmatrix} -\theta_0' \cos\theta_0(v' + \theta_0'u) \\ \cos\theta_0(v'' + \theta_0''u + \theta_0'u') - \sin\theta_0\theta_0'(v' + \theta_0'u) \end{Bmatrix} \tag{31}$$

and the beam slenderness ($\lambda := \ell/\sqrt{J/A}$) is introduced. The previous PDE boundary-value problem is completely defined with the following geometric and mechanical boundary conditions:

$$\begin{aligned} &u = 0,\ v = 0 \quad \text{at } x = 0, \\ &u = 0,\ v = 0 \quad \text{at } x = 1, \\ &v'' = 0 \quad \text{at } x = 0 \text{ and } 1. \end{aligned} \tag{32}$$

To formulate the eigenvalue problem, the two separable solutions $u(x,t) = U(x)e^{i\omega t}$ and $v(x,t) = V(x)e^{i\omega t}$ are introduced in Eq. (20), where the unknown mode shape functions $U(x)$ and $V(x)$ are both assumed as

$$\begin{Bmatrix} U(x) \\ V(x) \end{Bmatrix} \approx \sum_{k=1}^{M} \begin{Bmatrix} X_k \\ Y_k \end{Bmatrix} \sin(k\pi x). \tag{33}$$

The adopted trial sine functions are admissible, as they satisfy all of the boundary conditions. By introducing these expressions into the operators (29), (30) and (31) and applying the Galerkin procedure again, a set of $2M$ equations is obtained in the unknown coefficients X_k and Y_k. The discrete Galerkin equations are reported in Appendix B.

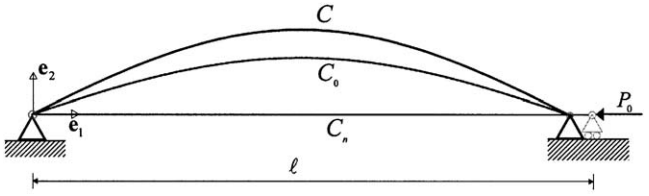

Fig. 2. Schematic geometry of the buckled beam with the stationary hinge in the post-buckling phase.

3. Numerical results and discussion

In this section, the main numerical results are discussed. First, the post-buckling solutions, obtained with the finite element code FEAP [28] and the perturbation expansion [20], are presented in Fig. 3 for a rectangular cross-section test beam with $\ell = 450\,\text{mm}$, $w_b = 10\,\text{mm}$, $t_b = 0.8\,\text{mm}$, $\rho = 8890\,\text{kg/m}^3$, $E = 106\,\text{GPa}$, where w_b and t_b denote the beam width and thickness, respectively. Consequently, the considered beam is rather slender, since $\lambda = 1948.6$. With the FEAP code, the beam is discretized using large displacement and large rotation two-node frame elements for two-dimensional geometries, based on the exact kinematic formulation of Simo and Vu-Quoc [29,30]. As to the nonlinear static analysis, a numerical step-by-step technique is employed applying the external load in a sequence of discrete time intervals characterized by a constant step. At each step, the solution is determined via a classical Newton–Raphson algorithm. As to the free vibration analysis, the natural frequencies and the associated mode shapes are evaluated by using the subspace iteration method.

To obtain the post-buckling solution, a very small initial imperfection is given, consisting of an initially curved rest configuration, instead of a perfectly straight configuration, with a sag-to-span ratio of about 10^{-6}. As clear in Fig. 3, there is a close agreement between the semi-analytical and numerical solutions, also for high loads up to two-and-a-half times the buckling load. Next, the main results regarding the linear vibration analysis are presented for the simply supported beam, when $\mu = 8.13$. Twelve trial functions are used in the semi-analytical approach, whereas a discretization with 100 elements is employed in the finite element computations for an overall number of 300 degrees of freedom.

In Fig. 4, the lowest six natural non-dimensional frequencies are shown in the pre- and post-buckling ranges. The dashed vertical line corresponds to the non-dimensional buckling load ($P_0^* = \pi^2$), whereby the frequency of the first mode vanishes (see also Fig. 5). Past the buckling load, the first frequency mildly increases, whereas the frequencies of the other modes slowly

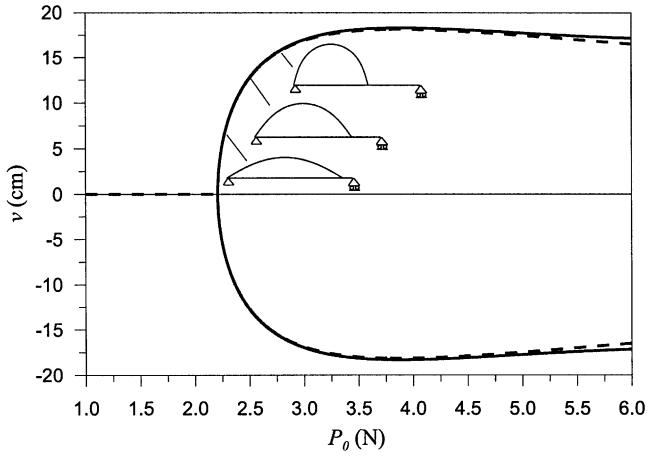

Fig. 3. Bifurcation diagram: variation of the deflection of the midspan section with the end load. The continuous (dashed) line indicates the analytical (numerical) solution.

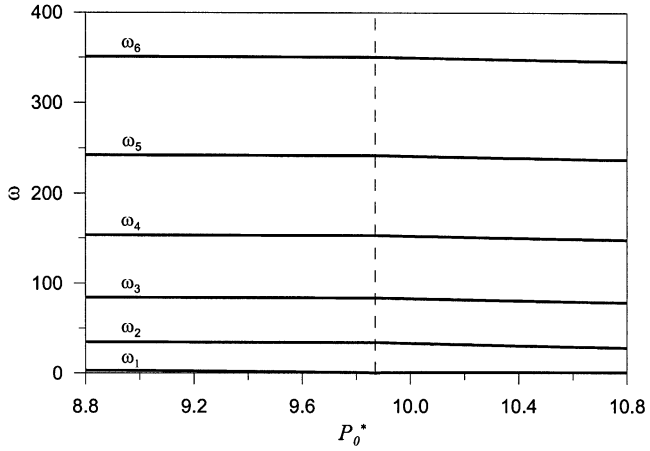

Fig. 4. Variation of the lowest six non-dimensional natural frequencies with the end load for the simply supported buckled beam.

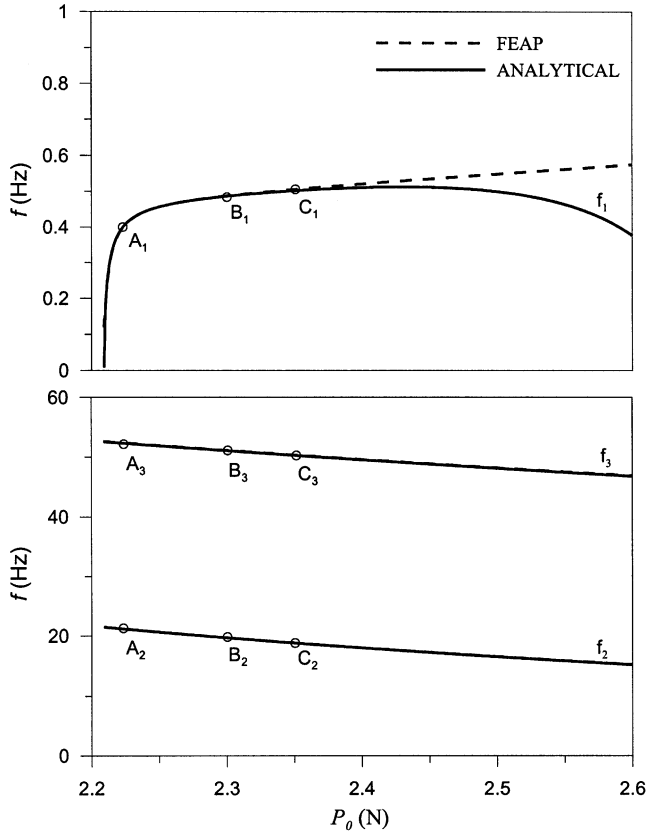

Fig. 5. Variation of the lowest three natural frequencies of the test simply supported beam with the end load: comparison between the analytical (continuous line) and numerical (dashed line) solutions.

decrease due to the overall stiffness drop caused by the negative geometric stiffness. No crossovers occur and the frequencies are well separated.

In Fig. 5, the lowest three-dimensional natural frequencies of the mentioned test beam can be more closely observed. In the top figure, it is worth noting that the agreement between the results obtained with the FEAP code and the Galerkin procedure for the first mode is very good up to 2.4 N (about 10% of the buckling load); thereafter, a deviation is observed due to the approximation in the post-buckling analytical static solution (the rotation field θ_0 is truncated to fifth order) and its consequences on the elastic and geometric stiffnesses. On the other hand, the higher frequencies agree very well, as they are less sensitive to the initial post-buckling curvature and pre-stress.

Further, it is interesting to note that the frequency of the first mode experiences a sharp growth in a very narrow load range right above the buckling load, whereas, subsequently, it increases with a much smaller rate. This is due to the fact that the growth of the beam stiffness from zero is very high past the buckling condition. The agreement between the numerically obtained results and the semi-analytical solutions is good also for the associated mode shapes calculated at the loads marked by A_k, B_k, and C_k, for the lowest three modes in Fig. 5 and shown, for the lowest six modes, in Fig. 6. It is worth observing that the first mode (first row in Fig. 6), as expected, entails a visible motion of the sliding hinge, hence of the end mass, whereas the higher modes are not affected by an appreciable motion of the boundary. Consequently, the first mode shape is not symmetric, whereas the higher modes are close to being symmetric and antisymmetric. Slight variations in the mode shapes are observed in the three pre-stressed conditions.

It is also interesting to investigate the dependence of the frequencies on the ratio between the end mass and the beam mass. In Fig. 7, the ratio ω/ω_0 is shown, where ω indicates the non-dimensional frequencies of the beam possessing the boundary mass and ω_0 denotes the frequencies of the beam without the boundary mass. As expected, the frequency of the first mode decreases significantly with increase in μ, up to a 70% decrease, when $\mu = 10$. On the other hand, the frequencies of the higher modes are less sensitive to the boundary mass. To study in closer detail the difference between the considered case of boundary mass ($\mu = 8.13$) and the case without end mass ($\mu = 0$), the non-dimensional frequency variation with the end load is computed and is shown in Fig. 8. Of course, there is no dependence on the pre-buckling range where the transverse bending modes of the straight beam are uncoupled from the axial modes, hence it does not imply horizontal motion of the boundary mass. In the post-buckling range, there is an increasing dependence with the end load. In particular, with an end load about 8% higher than the buckling load, the frequencies of the first and second modes of the beam without end mass are, respectively, 80% and 12% higher than the corresponding frequencies with the end mass.

Next, the results concerning the hinged–hinged buckled beam are shown and discussed. The first mode is expected to be dominated by the stretching effect. Figs. 9 and 10 show the lowest three and lowest five natural frequencies, respectively. In Fig. 9, the diamonds, stars and dots represent the frequencies calculated with the FEAP code and they closely match those computed with the semi-analytical method. The frequency of the first symmetric mode exhibits a sharp increase in the selected load range, as more clearly seen in Fig. 10. This steep growth of the first frequency is responsible for the observed four consecutive crossovers with the frequencies of the first antisymmetric, second symmetric, second antisymmetric and third symmetric modes. In this figure, A indicates antisymmetric mode shapes and S denotes symmetric mode shapes. These

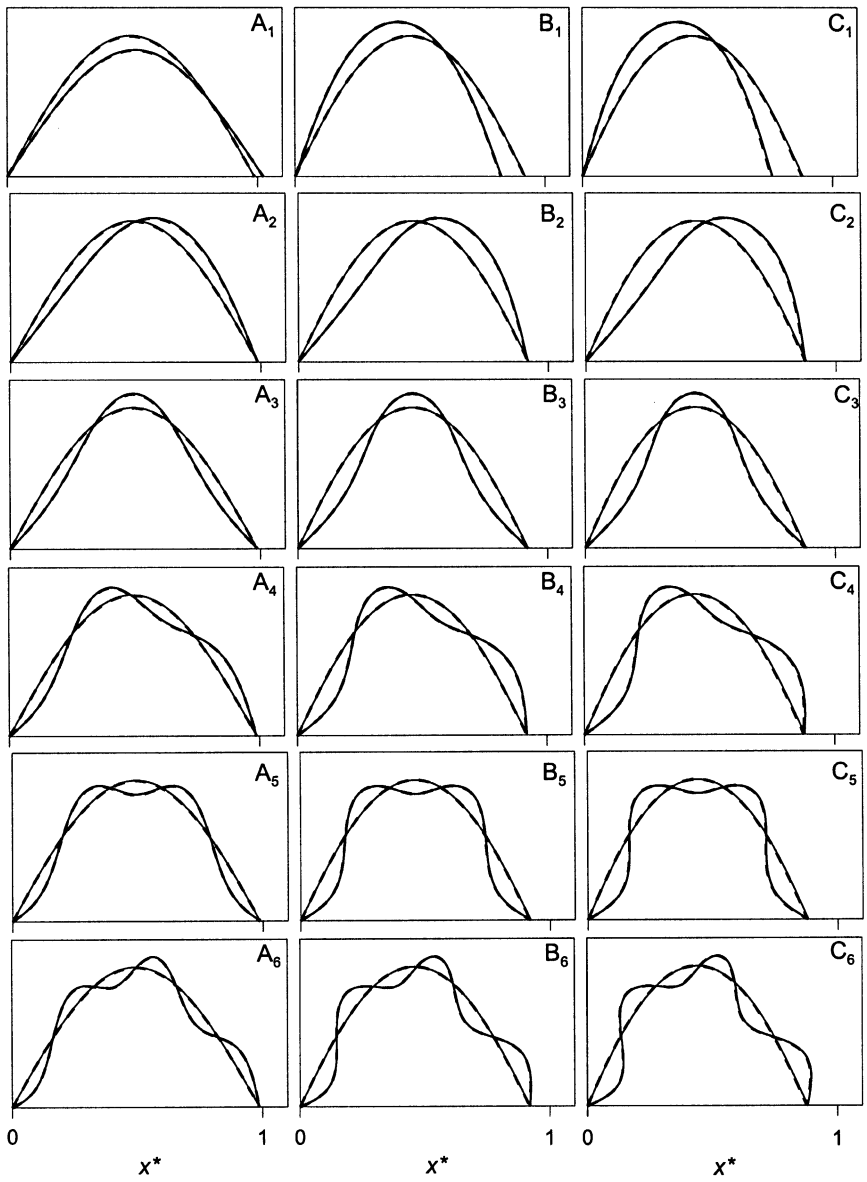

Fig. 6. Comparison between the analytical (continuous line) and numerical (dashed line) lowest six mode shapes at three different values of the end load for the simply supported buckled beam.

results agree with the results of Perkins [15], but for the first mode, which was not shown along with the crossovers. The remarkable feature is that these crossovers are all packed in a very narrow load range. Therefore, a very small load variation can cause sensibly different dynamic behaviors within this region. As well known, these crossovers entail one-to-one auto-parametric exchange of energy in the nonlinear vibration regime. In Fig. 9, two distinct crossovers are clearly discernible and are separated by an infinitesimal load increase (note the load scale in Fig. 9).

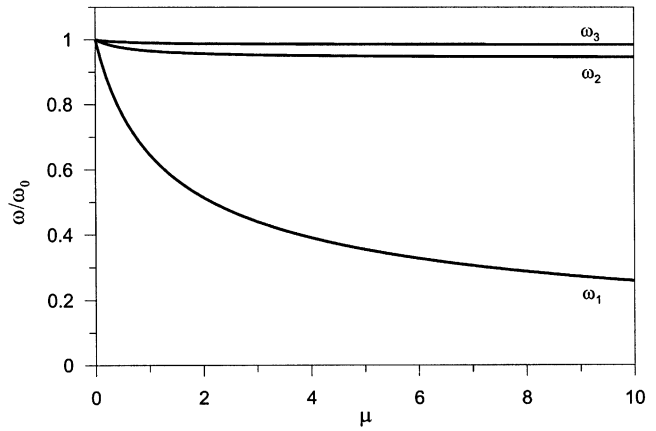

Fig. 7. Variation of the non-dimensional three lowest natural frequencies with the end mass in the case of sliding hinge post-buckling configuration.

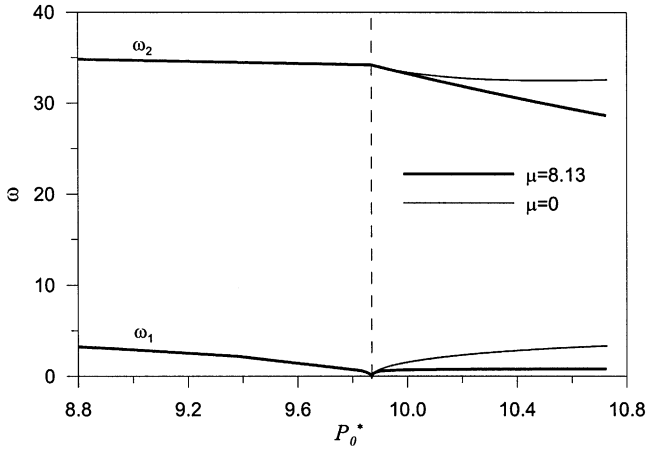

Fig. 8. Variation of the first and second natural frequencies with the end load with and without the end mass in the case of sliding hinge post-buckling configuration.

The finite element and the Galerkin solutions are in very good agreement also for the lowest six mode shapes calculated at the loads marked by A_k, B_k, and C_k, in Fig. 9 and shown in Fig. 11. We note that, because of the full symmetry in the boundary conditions, the mode shapes are symmetric and antisymmetric. The selected loads are located below the first crossover, between the first and second crossovers, and above the second crossover, respectively. Below the first crossover, the first mode is the symmetric stretching–bending mode, between the first and second crossovers, the lowest mode is the first antisymmetric bending mode, whereas the second mode is the symmetric stretching–bending mode. Above the second crossover, the lowest mode is still the first antisymmetric bending mode, whereas the second mode is the second symmetric bending mode (two nodes) and the third mode is the symmetric stretching–bending mode.

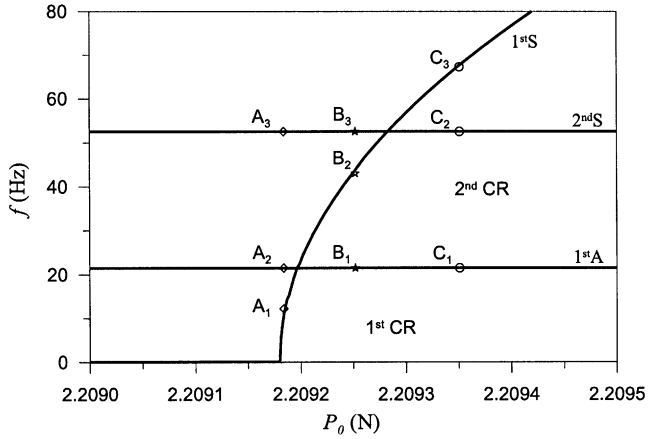

Fig. 9. Variation of the lowest three natural frequencies with the end load for the hinged–hinged configuration: comparison between the analytical (continuous line) and numerical (symbols) solutions.

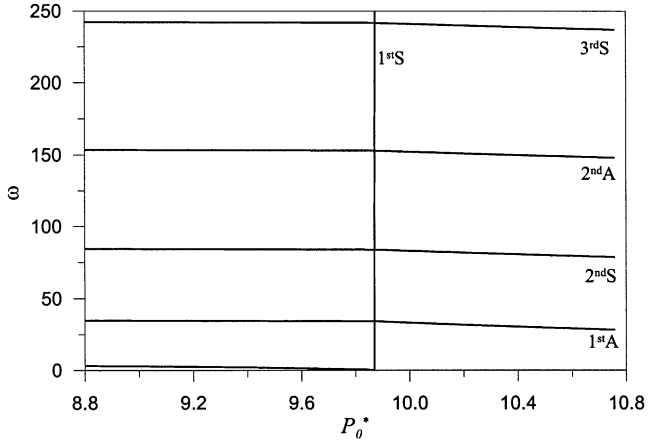

Fig. 10. Variation of the lowest five non-dimensional natural frequencies with the end load for the hinged–hinged post-buckled beam.

It is useful to compare the lowest two frequencies of the simply supported and hinged–hinged beams to show the influence of the different deformation mechanisms on the linear vibration response. Namely, in the second case, the dynamic stretching-induced stiffness overpowers the elastic bending stiffness and causes a sharp increase of the fundamental frequency associated with a symmetric shape. In the simply supported case, this mechanism is not activated and the stiffness is primarily due to the bending deformation process. The variation of the frequencies in Fig. 12 clearly shows this mechanical behavior.

The strong variation of the frequency of the stretching–bending mode with the load deserves some further comments. Looking closely at the balance equation in the transverse direction, Eq. (11_2), we note that the load-carrying mechanisms are related to the bending process, expressed

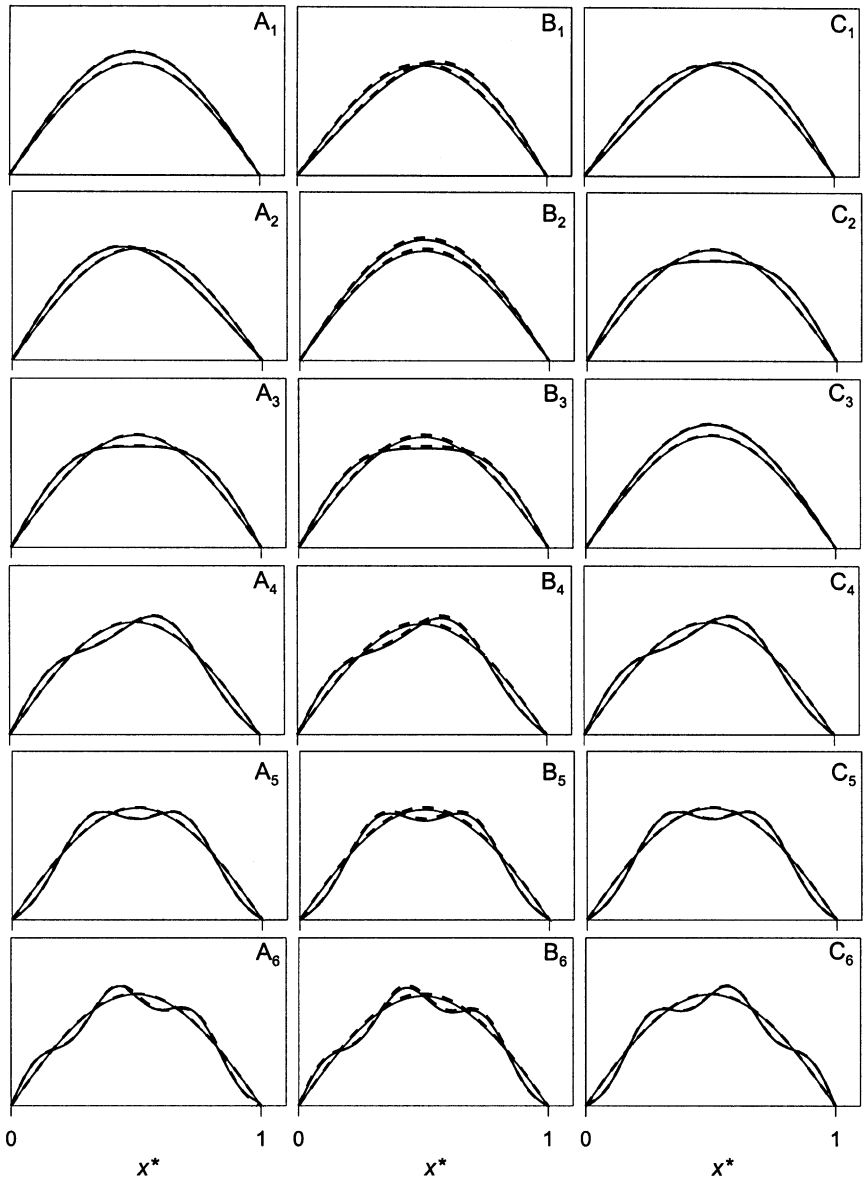

Fig. 11. Comparison between the analytically obtained (continuous line) and the numerically obtained (dashed line) first six mode shapes at three different values of the end load for the hinged–hinged beam.

by M'', and to the stretching mechanism (also known as *funicular* load-carrying mechanism), expressed by the term $-\kappa_0 N$. The other forces appearing in the balance equations, $-(N_0\kappa + N_0'\theta)$, are due to the pre-stress and act as *de-stabilizing* forces. The overall restoring forces, besides that due to bending, are the summation of the stretching forces and the de-stabilizing forces arising from the pre-stress. The stretching load-carrying effect depends quadratically on the initial curvature, because the stretching axial force depends on the initial curvature (see the

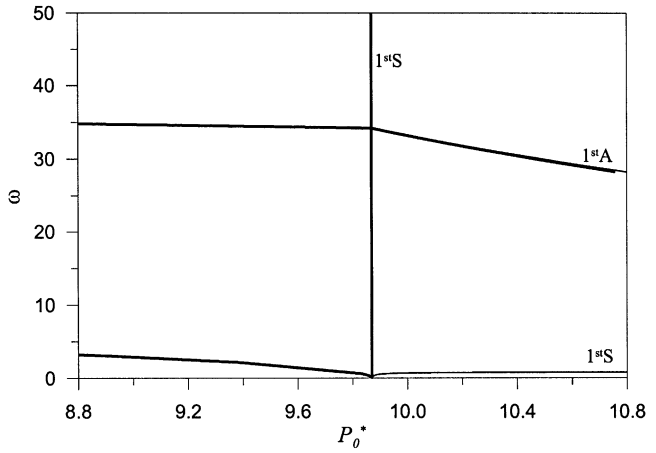

Fig. 12. The lowest two frequencies of the simply supported (thin line) and hinged–hinged (thick line) buckled beams.

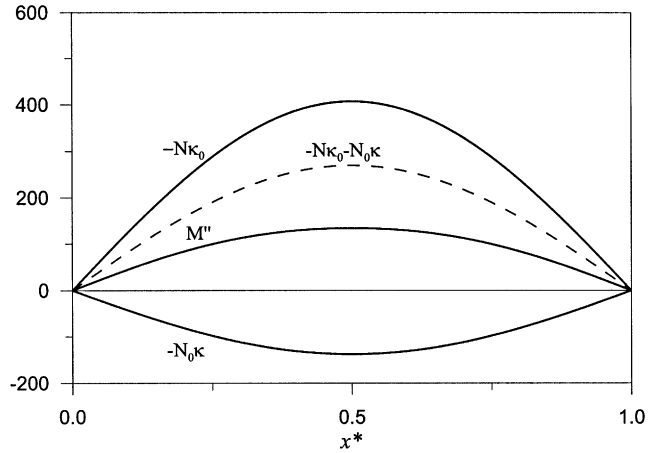

Fig. 13. Variation of the different load-carrying forces along the beam axis for the end load level corresponding to A_k in Fig. 9.

definition of ε) and is multiplied by the initial curvature itself. Overall, the dependence of the frequency of the stretching–bending mode with the load is at least quadratic. To outline the relative importance of the bending and stretching effects, Figs. 13 and 14 show variations of these terms with x^* when the end load level is at A_k and B_k, respectively (see Fig. 9). Clearly, the mode right above buckling and below the first crossover is a stretching–bending mode, as the load-carrying terms are of the same orders. On the other hand, past the first crossover, the mode becomes a truly stretching mode, as the overall stretching restoring forces are three orders of magnitude greater than the bending force.

It is also worth investigating the dependence of the frequencies on the beam slenderness. A beam about two orders of magnitude less slender is considered, namely with $\lambda = 31.62$, and the

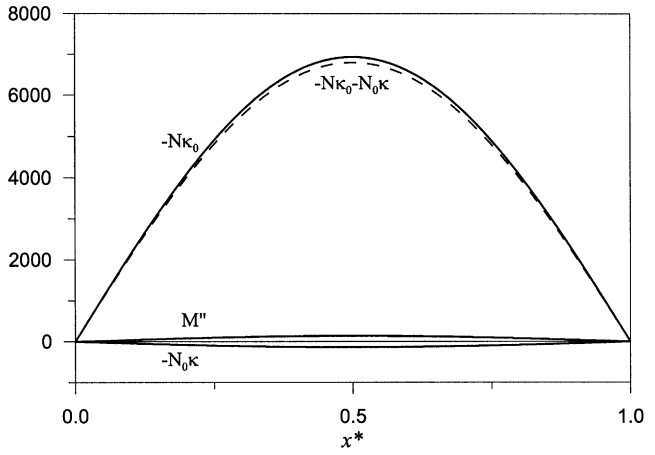

Fig. 14. Variation of the different load-carrying forces along the beam axis for the end load level corresponding to B_k in Fig. 9.

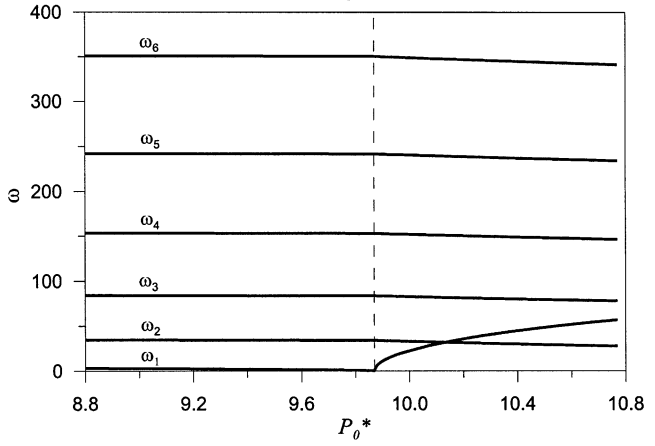

Fig. 15. Variation of the lowest natural frequencies with the end load in the case of hinged–hinged post-buckling configuration for $\lambda = 31.62$.

variation of the lowest six frequencies with the end load is shown in Fig. 15. In this case, the bending load-carrying capability is not overpowered by the funicular load-carrying capability. Hence, the increase in the frequency of the first mode with the load is milder than in the case of the more slender beam. In the same load range, the frequency of the first mode of the beam with $\lambda = 31.62$ experiences only one crossover with the frequency of the first antisymmetric mode. In order to confirm this, the switch between the mode shapes of the lowest two modes at the crossover is shown in Fig. 16.

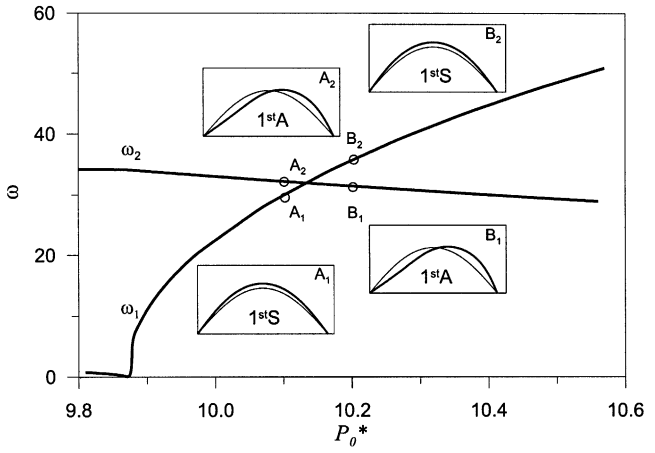

Fig. 16. Zoom on the first and second natural frequencies with the end load in the case of hinged–hinged post-buckling configuration for $\lambda = 31.62$ and the associated mode shapes.

4. Conclusions

In this paper, the leading features of the unforced undamped linear vibrations of buckled beams are computed and discussed, investigating the dependence of the natural frequencies and mode shapes on the end load (i.e., the pre-stress level). The solutions obtained with a Galerkin formulation, using appropriate admissible functions and an asymptotic expansion of the post-buckling solution, have been compared with a finite-element formulation. In general, it was found that the finite-element implementation required a rather fine mesh to match closely the result obtained with the Galerkin formulation.

Distinguished differences have been found between the linear dynamic behavior of the simply supported inextensible beam and that of the hinged–hinged beam (in the post-buckling), whereby the beam undergoes stretching and bending deformation modes. Specifically, in the first case, the modes are bending modes and their frequencies are well separated, whereas, in the second case, the first mode is primarily a stretching mode and its frequency undergoes crossovers with those of the other modes with unappreciable load increases. This sharp difference in the linear vibration signatures of the two differently constrained beams is expected to become more dramatic in the nonlinear range, where the second system may experience coupled stretching–bending mode interaction at the crossovers.

Acknowledgements

This work was partially supported by a FY-2001 Grant "*Giovani Ricercatori*" (Young Investigators) and a FY-2002-03 Faculty of Engineering Grant sponsored by the University of Rome La Sapienza.

Appendix A. Simply supported beam

The function $y_k(x)$ must satisfy the following boundary conditions:
at $x = 0$:

$$\sum_{k=1}^{M} X_k y_k(x) = 0, \quad \sum_{k=1}^{M} X_k y_k''(x) = 0.$$

at $x = 1$:

$$\sum_{k=1}^{M} X_k \left\{ y_k(x) + \tan\theta_0 \left[\int_0^x \theta_0' (\sin(k\pi x) + y_k(x))\,\mathrm{d}x \right] \right\} = C_{1,k},$$

$$\sum_{k=1}^{M} X_k \left\{ y_k''(x) + \tan\theta_0'' \left[\int_0^x \theta_0' (\sin(k\pi x) + y_k(x))\,\mathrm{d}x \right] \right\} = C_{2,k}.$$

The function $y_k(x)$ may be expressed by a third-order polynomial. By letting

$$y_k(x) = a_{0,k} + a_{1,k}x + a_{2,k}x^2 + a_{3,k}x^3,$$

the first two boundary conditions at $x = 0$ lead to

$$a_{0,k} = 0, \quad a_{1,k} = C_{1,k} - \tfrac{1}{6}C_{2,k}, \quad a_{2,k} = 0, \quad a_{3,k} = \tfrac{1}{6}C_{2,k}$$

and

$$y_k(x) = \left(C_{1,k} - \frac{C_{2,k}}{6} \right) x + \frac{C_{2,k}}{6}\, x^3.$$

By substituting the expression of $y_k(x)$ into the last two boundary conditions at $x = 1$, the constants $C_{i,k}$ are determined as the solution of the resulting set of equations in the form

$$C_{1k} = \frac{\hat{\theta}_0 \pi}{D} \left\{ -432{,}000 \tan\left(\hat{\theta}_0 - \tfrac{1}{192}\hat{\theta}_0^3 + \tfrac{1}{5120}\hat{\theta}_0^5 \right) \times \left[4096\delta_{1k} + (3\hat{\theta}_0^4 - 64\hat{\theta}_0^2)\delta_{3k} - \hat{\theta}_0^4 \delta_{5k} \right] \right\},$$

$$C_{2k} = \frac{1}{8D} \left\{ 3375\hat{\theta}_0^2 \pi^3 (1024 - 48\hat{\theta}_0^2 + \hat{\theta}_0^4) \times \left[4096\delta_{1k} + (3\hat{\theta}_0^4 - 64\hat{\theta}_0^2)\delta_{3k} - \hat{\theta}_0^4 \delta_{5k} \right] \right\},$$

where δ_{ij} is the Kronecker delta and

$$D = 3538{,}944{,}000(1+\hat{\theta}_0^2) - 167{,}936{,}000\hat{\theta}_0^4 + 3641{,}088\hat{\theta}_0^6 - 6176\hat{\theta}_0^8 + 87\hat{\theta}_0^{10} + 230{,}400\hat{\theta}_0(15{,}360 - 80\hat{\theta}_0^2 + 3\hat{\theta}_0^4)\tan\left(\hat{\theta}_0 - \tfrac{1}{192}\hat{\theta}_0^3 + \tfrac{1}{5120}\hat{\theta}_0^5\right).$$

The discretized expressions of the inertial and stiffness operators are

$$\mathscr{I}_j = \sum_{k=1}^{M} X_k\left(-B_{jk} - C_{jk} + \frac{2\mu}{\sin 2\theta_0(1)} D_{jk}\right),$$

$$\mathscr{L}_{Ej} = \sum_{k=1}^{M} X_k(E_{jk} + F_{jk} + G_{jk} + H_{jk} + I_{jk} + J_{jk} + L_{jk} + N_{jk} - O_{jk} - P_{jk} - Q_{jk} - R_{jk}),$$

$$\mathscr{L}_{Gj} = \sum_{k=1}^{M} X_k(S_{jk} - T_{jk} - U_{jk} - V_{jk} - W_{jk} + X_{jk} + Y_{jk} + Z_{jk}),$$

$$B_{jk} = \int_0^1 f_j^* f_k \,\mathrm{d}x, \qquad C_{jk} = \int_0^1 f_j^* \theta_0' \left[\int_x^1 \left(\int_0^\eta \theta_0' f_k \,\mathrm{d}\xi\right)\mathrm{d}\eta\right]\mathrm{d}x,$$

$$D_{jk} = \int_0^1 f_j^* \theta_0' \left(\int_0^1 \theta_0' f_k \,\mathrm{d}x\right)\mathrm{d}x, \qquad E_{jk} = \int_0^1 f_j^* f_k'''' \,\mathrm{d}x,$$

$$F_{jk} = \int_0^1 f_j^* \theta_0'''' \left(\int_0^x \theta_0' f_k \,\mathrm{d}\eta\right)\mathrm{d}x, \qquad G_{jk} = \int_0^1 f_j^* 4\theta_0'\theta_0''' f_k \,\mathrm{d}x,$$

$$H_{jk} = \int_0^1 f_j^* 3\theta_0''^2 f_k \,\mathrm{d}x, \qquad I_{jk} = \int_0^1 f_j^* 5\theta_0'\theta_0'' f_k' \,\mathrm{d}x,$$

$$J_{jk} = \int_0^1 f_j^* \theta_0'^2 f_k'' \,\mathrm{d}x, \qquad L_{jk} = \int_0^1 f_j^* \theta_0' \tan\theta_0(1) f_k'''(1)\,\mathrm{d}x,$$

$$N_{jk} = \int_0^1 f_j^* \theta_0' \tan\theta_0(1)\theta_0'''(1)\left(\int_0^1 \theta_0' f_k \,\mathrm{d}x\right)\mathrm{d}x, \qquad O_{jk} = \int_0^1 f_j^* \theta_0' \left(\int_x^1 \theta_0' f_k''' \,\mathrm{d}\eta\right)\mathrm{d}x,$$

$$P_{jk} = \int_0^1 f_j^* \theta_0' \left[\int_x^1 \theta_0'\theta_0''' \left(\int_0^\eta \theta_0' f_k \,\mathrm{d}\xi\right)\mathrm{d}\eta\right]\mathrm{d}x, \qquad Q_{jk} = \int_0^1 f_j^* \theta_0' \left(\int_x^1 3\theta_0'^2\theta_0'' f_k \,\mathrm{d}\eta\right)\mathrm{d}x,$$

$$R_{jk} = \int_0^1 f_j^* \theta_0' \left(\int_x^1 \theta_0'^3 f_k' \,\mathrm{d}\eta\right)\mathrm{d}x, \qquad S_{jk} = \int_0^1 f_j^* \theta_0' f_k'(1)\sin\theta_0(1)\,\mathrm{d}x,$$

$$T_{jk} = \int_0^1 f_j^* \theta_0' \left(\int_x^1 \theta_0' \cos\theta_0 f_k' \,\mathrm{d}\eta\right)\mathrm{d}x, \qquad U_{jk} = \int_0^1 f_j^* \theta_0' \left[\int_x^1 \theta_0'^2 \cos\theta_0 \left(\int_0^\eta \theta_0' f_k \,\mathrm{d}\xi\right)\mathrm{d}\eta\right]\mathrm{d}x,$$

$$V_{jk} = \int_0^1 f_j^* \theta_0' \sin\theta_0 f_k' \,\mathrm{d}x, \qquad W_{jk} = \int_0^1 f_j^* (\theta_0')^2 \sin\theta_0 \left(\int_0^x \theta_0' f_k \,\mathrm{d}\eta\right)\mathrm{d}x,$$

$$X_{jk} = \int_0^1 f_j^* \cos\theta_0 f_k'' \,\mathrm{d}x, \qquad Y_{jk} = \int_0^1 f_j^* \cos\theta_0 \theta_0'' \left(\int_0^x \theta_0' f_k \,\mathrm{d}\eta\right)\mathrm{d}x,$$

$$Z_{jk} = \int_0^1 f_j^* \cos\theta_0 \theta_0'^2 f_k \,\mathrm{d}x,$$

having denoted with $f_k(x)$ the expression

$$f_x(x) = f_k^*(x) = \sin(k\pi x) + y_k(x).$$

Appendix B. Hinged–hinged beam

The discretized expressions of the inertial and stiffness operators are

$$\mathbf{I}_j = -\sum_{k=1}^{M} \begin{Bmatrix} X_k \\ Y_k \end{Bmatrix} C_{jk},$$

$$\mathbf{L}_{Ej} = \begin{cases} \sum_{k=1}^{M} [X_k(-\lambda^2 D_{jk} - E_{jk} - F_{jk} - 2G_{jk}) + Y_k(\lambda^2 H_{jk} + \lambda^2 I_{jk} - J_{jk})], \\ \sum_{k=1}^{M} [X_k(-\lambda^2 I_{jk} + J_{jk} + L_{jk} + 3N_{jk} + 3O_{jk}) + Y_k(P_{jk} + \lambda^2 Q_{jk})], \end{cases}$$

$$\mathbf{L}_{Gj} = \begin{cases} \sum_{k=1}^{M} [X_k(-R_{jk}) + Y_k(-S_{jk})], \\ \sum_{k=1}^{M} [X_k(S_{jk} + T_{jk} - U_{jk}) + Y_k(V_{jk} - W_{jk})], \end{cases}$$

where

$$C_{jk} = \int_0^1 f_j^* f_k \, \mathrm{d}x, \quad D_{jk} = \int_0^1 f_j^* f_k'' \, \mathrm{d}x, \quad E_{jk} = \int_0^1 f_j^* (\theta_0')^2 f_k'' \, \mathrm{d}x,$$
$$F_{jk} = \int_0^1 f_j^* \theta_0' \theta_0''' f_k \, \mathrm{d}x, \quad G_{jk} = \int_0^1 f_j^* \theta_0' \theta_0'' f_k' \, \mathrm{d}x, \quad H_{jk} = \int_0^1 f_j^* \theta_0'' f_k \, \mathrm{d}x,$$
$$I_{jk} = \int_0^1 f_j^* \theta_0' f_k' \, \mathrm{d}x, \quad J_{jk} = \int_0^1 f_j^* \theta_0' f_k''' \, \mathrm{d}x, \quad L_{jk} = \int_0^1 f_j^* \theta_0'''' f_k \, \mathrm{d}x,$$
$$N_{jk} = \int_0^1 f_j^* \theta_0''' f_k' \, \mathrm{d}x, \quad O_{jk} = \int_0^1 f_j^* \theta_0'' f_k'' \, \mathrm{d}x, \quad P_{jk} = \int_0^1 f_j^* f_k'''' \, \mathrm{d}x,$$
$$Q_{jk} = \int_0^1 f_j^* (\theta_0')^2 f_k \, \mathrm{d}x, \quad R_{jk} = \int_0^1 f_j^* \cos\,\theta_0 \theta_0'^2 f_k \, \mathrm{d}x, \quad S_{jk} = \int_0^1 f_j^* \cos\,\theta_0 \theta_0' f_k' \, \mathrm{d}x,$$
$$T_{jk} = \int_0^1 f_j^* \cos\theta_0 \theta_0'' f_k \, \mathrm{d}x, \quad U_{jk} = \int_0^1 f_j^* \sin\,\theta_0 \theta_0'^2 f_k \, \mathrm{d}x, \quad V_{jk} = \int_0^1 f_j^* \cos\,\theta_0 f_k'' \, \mathrm{d}x,$$
$$W_{jk} = \int_0^1 f_j^* \sin\theta_0 \theta_0' f_k' \, \mathrm{d}x,$$

having denoted with $f_k(x)$ the expression

$$f_k(x) = f_k^*(x) = \sin(k\pi x).$$

References

[1] P. Chidamparam, A.W. Leissa, Vibration of planar curved beams, rings, and arches, *Applied Mechanics Review* 46 (1993) 467–483.

[2] P.A.A. Laura, M.J. Maurizi, Recent research on vibrations of arch-type structures, *Shock and Vibration Digest* 19 (1987) 6–9.

[3] J.P. Den Hartog, The lowest frequency of circular arcs, *Philosophical Magazine* 5 (1928) 400–408.
[4] S.S. Rao, V. Sundararajan, In-plane flexural vibrations of circular rings, *Journal of Applied Mechanics* 36 (1969) 620–625.
[5] E. Tufekci, A. Arpaci, Exact solution of in-plane vibrations of circular arches with account taken of axial extension, transverse shear and rotatory inertia effects, *Journal of Sound and Vibration* 209 (1998) 845–856.
[6] P. Chidamparam, A.W. Leissa, Influence of centerline extensibility on the in-plane free vibrations of loaded circular arches, *Journal of Sound and Vibration* 183 (1995) 779–795.
[7] S.T. Mau, A.N. Williams, Green's function solution for arch vibration, *Journal of Engineering Mechanics* 114 (1988) 1259–1264.
[8] M. Petyt, C.C. Fleischer, Free vibration of a curved beam, *Journal of Sound of Vibration* 18 (1971) 17–30.
[9] G. Prathap, The curved beam/deep arch/finite ring element revisited, *International Journal for Numerical Methods in Engineering* 21 (1985) 389–497.
[10] S.Y. Yang, H.C. Sin, Curvature-based beam elements for the analysis of Timoshenko and shear-deformable curved beams, *Journal of Sound and Vibration* 187 (1995) 569–584.
[11] K. Grosh, P.M. Pinsky, In-plane vibration and stability of shallow circular arches subjected to axial forces, *Computer Methods in Applied Mechanics and Engineering* 132 (1996) 1–16.
[12] K.J. Kang, C.W. Bert, A.G. Striz, Vibration and buckling analysis of circular arches using DQM, *Computers and Structures* 60 (1996) 49–57.
[13] K. Matsunaga, In-plane vibration and stability of shallow circular arches subjected to axial forces, *International Journal of Solids and Structures* 33 (1996) 469–482.
[14] S.-J. Oh, B.K. Lee, I.-W. Lee, Free vibrations of non-circular arches with non-uniform cross-section, *International Journal of Solids and Structures* 37 (2000) 4871–4891.
[15] N.C. Perkins, Planar vibration of an elastic arch: theory and experiment, *Journal of Vibration and Acoustics* 112 (1990) 374–379.
[16] E. Mettler, *Dynamic Buckling in Handbook of Engineering Mechanics*, McGraw-Hill, New York, 1962.
[17] A.H. Nayfeh, W. Kreider, T.J. Anderson, Investigation of natural frequencies and mode shapes of buckled beams, *AIAA Journal* 33 (1995) 1121–1126.
[18] W. Lacarbonara, A.H. Nayfeh, W. Kreider, Experimental validation of reduction methods for weakly nonlinear distributed-parameter systems: analysis of a buckled beam, *Nonlinear Dynamics* 17 (1998) 95–117.
[19] P. Villaggio, *Mathematical Models for Elastic Structures*, Cambridge University Press, Cambridge, 1997.
[20] W. Lacarbonara, A. Paolone, H. Yabuno, Parametric resonances of planar pre-stressed curved beams, *ICIAM 2003*, *5th International Congress on Industrial and Applied Mathematics*, Sydney, Australia, July 7–11, 2003.
[21] J. Winterflood, T. Barber, B. Slagmolen, High performance vibration isolation using spring in Euler column buckling mode, *Physics Letters A* 300 (2002) 122–130.
[22] L.N. Virgin, R.B. Davis, Vibration isolation using buckled structures, *Journal of Sound and Vibration* 260 (2003) 965–973.
[23] J. Jiang, E. Mockensturm, A novel motion amplifier using an axially driven buckling beam, *ASME International Mechanical Engineering Congress and RD&D Exposition*, Washington, DC, USA, November 15–21, 2003.
[24] W. Lacarbonara, A. Paolone, H. Yabuno, Modeling of planar nonshallow prestressed beams towards asymptotic solutions, *Mechanics Research Communications* 31 (2004) 301–310.
[25] B.A. Finlayson, *The Method of Weighted Residuals and Variational Principles*, Academic Press, New York, 1972.
[26] S.P. Timoshenko, J.M. Gere, *Theory of Elastic Stability*, McGraw Hill, New York, 1961.
[27] A. Magnusson, M. Ristinmaa, C. Ljung, Behaviour of the extensible elastica solution, *International Journal of Solids and Structures* 38 (2001) 8441–8457.
[28] R.L. Taylor, *FEAP—a finite element analysis program,* Version 7.4, Department of Civil and Environmental Engineering, University of California, Berkeley, CA, 2002.
[29] J.C. Simo, L. Vu-Quoc, A three-dimensional finite strain rod model—part II: geometric and computational aspects, *Computer Methods in Applied Mechanics and Engineering* 58 (1986) 79–116.
[30] J.C. Simo, L. Vu-Quoc, On the dynamics in space of rods undergoing large motions—a geometrically exact approach, *Computer Methods in Applied Mechanics and Engineering* 66 (1988) 125–161.